Section 8

Development of and advances in ocean modelling and data assimilation, sea-ice modelling, wave modelling

On the Variability of the Mediterranean Outflow Water in North Atlantic HYCOM Simulations

Alexandra Bozec[1], Eric Chassignet[1], Susan Lozier[2], Zulema Garraffo[3] and George Halliwell[3]

[1] *Center for Ocean and Atmospheric Predictions studies, Tallahassee, Florida*
[2] *Duke University, Durham, North Carolina*
[3] *Rosenstiel School of Marine and Atmospheric Science, Miami, Florida*
abozec@coaps.fsu.edu

1. Introduction

Several questions remain unanswered about the role and importance of the Mediterranean Overflow Water (MOW) for the Atlantic Ocean circulation and the global thermohaline circulation. Of particular interest is the temporal variability of the MOW and the mechanism(s) responsible for such variability on interannual and decadal scales. The source of the MOW variability can be attributed to changes in the North Atlantic Central Water (NACW) entrained in the Gulf of Cadiz, changes in the source water (i.e. Mediterranean Sea water), or both.

Potter and Lozier (2004) analyzed the variability the MOW at the depth of 1150m from observations collected between 1955 and 1993 in the vicinity of the Gulf of Cadiz. They found a positive trend in both temperature (0.101 +/- 0.024ºC/decade) and salinity (0.0283+/- 0.0067psu/decade). More recently, Leadbetter et al. (2007), analyzing data from transects at 36ºN performed in 1959, 1981 and 2005 found a 20-year reversal in the water mass trends of MOW. This reversal trend consists in a warming and saltening of the MOW between 1959 and 1981, and a cooling and freshening between 1981 and 2005. Yet, the variability of the water in the western Mediterranean Sea shows weaker positive trend in the intermediate and deep layers till 2000 (0.035ºC/decade; 0.01psu/decade, Rixen et al. 2005) and higher trends in the last years (+0.30ºC/+0.02psu; Millot et al., 2006).

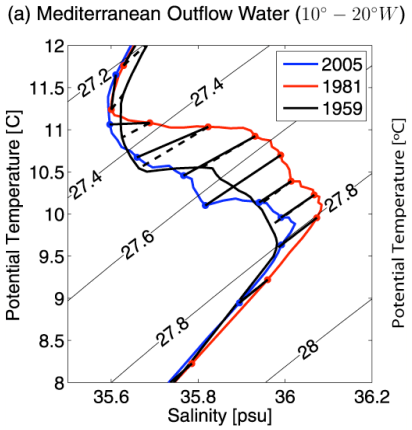

Figure 1: Mean observed θ/S profile of a section at 36ºN between 10º-20ºW at the depth of the MOW on neutral density (from Leadbetter et al., 2007).

2. Objectives and Method

In this study, we aim at determining the component(s) (i.e. Mediterranean Sea water or entrained NACW) responsible for the observed 20-year reversal trend. We use a 1/3º Atlantic configuration of the HYbrid Coordinate Ocean Model (HYCOM-http://www.hycom.org/) with the Price and Yang (1998) box model used as boundary condition for the Mediterranean outflow. A 56-year realistic experiment forced by NCEP interannual atmospheric fields (1948-2003) is performed to test the ability of the model to reproduce the observed variability. This interannual experiment is compared with a control experiment forced with climatological atmospheric fields. Each experiment starts from the same 20-year spin-up that uses the GDEM3 climatology as initial state. The northern and southern boundaries are treated as closed and the T/S values are relaxed toward the GDEM3 climatology. In the Price and Yang box model, the salt and heat budgets of the Mediterranean Sea are constant. Therefore, no variability of this marginal sea is introduced in the system.

3. Results

When compared to the observations, HYCOM presents a warmer and saltier Mediterranean tongue at 36ºN between 10º and 20ºW. However, the model succeeds in reproducing the variability observed by Leadbetter et al. (2007), showing that this 20-year reversal trend comes from the Atlantic Ocean and not from the Mediterranean Sea. The analysis of the results of the Price and Yang box model also shows that this variability results mostly from the variability of the entrained water (North Atlantic Central Water) in the Gulf of Cadiz (not shown). The comparison with the climatological run (Fig 2c) shows that the observed variability is not internal variability to the Atlantic Ocean or due to a model's drift but is actually by the atmospheric forcing.

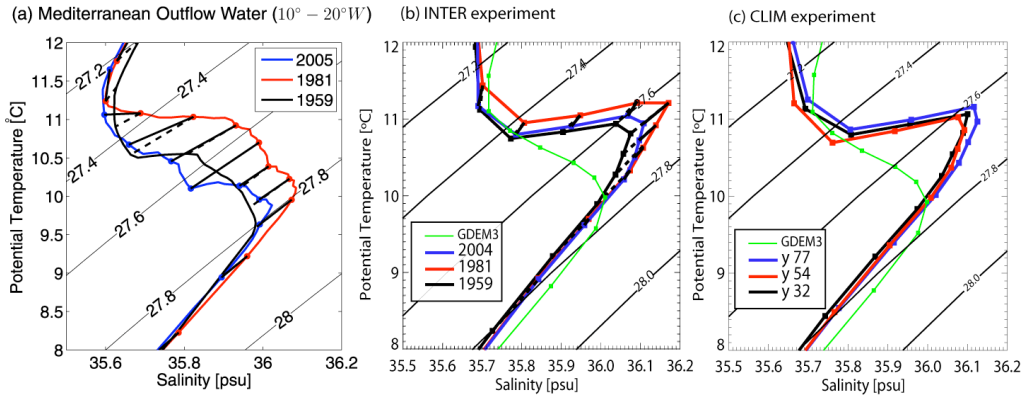

Figure 2: Mean θ/S profile of a section at 36ºN between 10º-20ºW at the depth of the MOW for a) observations (Leadbetter et al., 2007), b) for experiment INTER and c) experiment CLIM. The initial state (GDEM3) profile is plotted in green.

Acknowledgments.
This research was supported by the National Science Fondation through grant OCE-0630229.

References:

Leadbetter, S. J., Williams, R.J., McDonagh, E.L., King, B.A., 2007: A twenty year reversal in water mass trends in the subtropical North Atlantic, *Geophysical Research Letters,* **34**, doi:10.1029/2007GL029957.

Millot, C., 2006: Large warming and salinification of the Mediterranean outflow due to changes in its composition, Deep Sea Research I, 53, 656-666

Potter, R. A., Lozier, S.M., 2004: On the warming and salinification of the Mediterranean outflow waters in the North Atlantic, *Geophysical Research Letters,* **31**, L01202, doi:10.1029/2003GL018161.

Price, J.F. and J. Yang, 1998: Marginal sea overflows for climate simulations. In: *Ocean Modeling and Parameterizations*. E. P. Chassignet and J. Verron, Eds., Kluwer Acad. Pub., 155-170.

Rixen, M., Beckers, J.-M., Levitus, S., Antonov, J., Boyer, T., Maillard, C., Fichaut, M., Balopoulos, E., Iona, S., Dooley, H., Garcia, M.-J., Manca, B., Giorgetti, A., Manzella, G., Mikhailov, N., Pinardi, N., Zavatarelli,M., 2005: The Western Mediterranean Deep Water: a proxy for climate change, *Geophysical Research Letters,* **32**, doi:10.1029/205GL022702.

Western North Pacific SST Analyses based on Ship and Buoy Observations

Rick Danielson (@phys.ocean.dal.ca)
Oceanography, Dalhousie University, Halifax, Nova Scotia

The 1980s marked the beginning of multichannel infrared monitoring of SST from space and microwave observations have since become available as well. These data have permitted high spatial and temporal resolution analyses to be made (Reynolds et al. 2002), although for the period prior to the 1980s, SST analyses and observational summaries have generally been produced at one–month intervals (Rayner et al. 2003). This temporal limitation is one of many challenges in the search for systematic short–period interactions between the atmosphere and ocean. The objective of this work is to explore a simple method of interpolating not only *in situ* SST observations, but also measurement method, under the assumption that physical understanding is dependent on both.

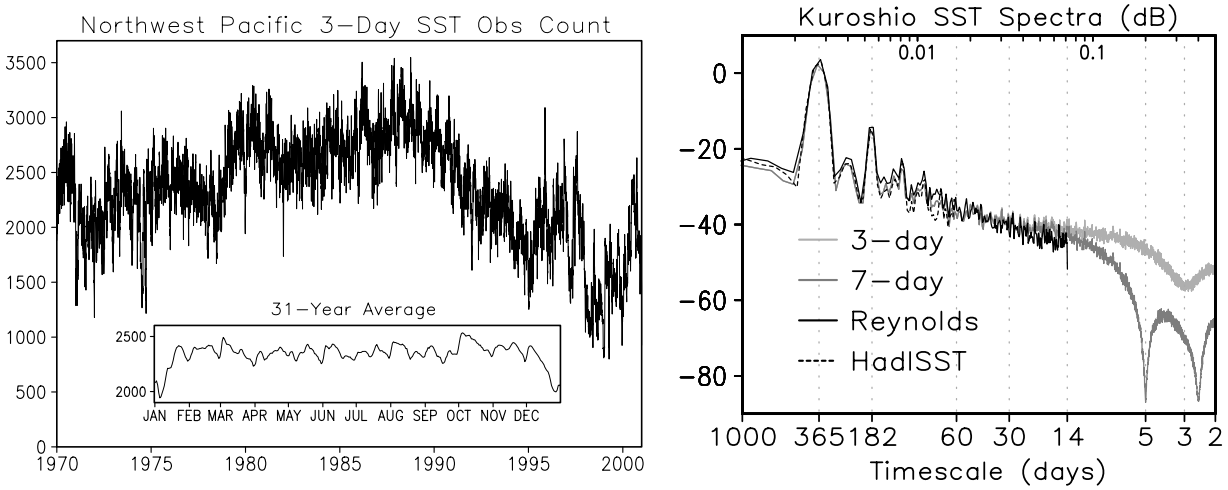

Figure 1: [Left] A 31–year (1970–2000) timeseries of the number of quality controlled ICOADS SST observations during consecutive three–day periods for the western North Pacific domain (shown in Fig. 2). A 31–year average for each day of the year is shown in the inset. [Right] Power spectral density (PSD) estimates of Kuroshio current extension SST variations during 1982–1989. These are based on timeseries of daily 3–day (light line) and 7–day (medium line) *in situ* analyses, weekly Reynolds analyses (dark line), and monthly HadISST analyses (dashed line). Each PSD estimate is an average of the local spectra within a $16^\circ \times 25^\circ$ box centered on the Kuroshio current extension. The ordinate is PSD in $^\circ C^2$ (cycles per day)$^{-1}$ and is expressed in dB.

The International Comprehensive Ocean–Atmosphere Data Set (ICOADS; Worley et al. 2005) is a compilation of the world's *in situ* surface marine observations. We consider only those ICOADS observations of high quality (i.e., within 2.8 estimated standard deviations of a smoothed monthly climatology). For the western North Pacific region, there are often more than 2000 observations during any three-day period (Fig. 1), with fewer observations at the end of December and beginning of January (see inset), presumably owing to the working schedules of voluntary observing ships.

The feasibility of a simple analysis for one three–day period with only 810 observations is given in Fig. 2. Here, a simple two–step analysis scheme is employed, where the first step defines a gridded value as a weighted average of the 15^{th} nearest observation and a spatially variable influence radius is employed. This step has a well known bias (Daley 1991) that results from an uneven distribution of influential observations perpendicular to the strong SST gradient (inside the oval). We thus calculate a weighted average for positional displacement in the same way that the weighted average for SST is obtained. This yields an unstructured grid, from which we obtain gridded SST values by Delaunay triangulation and interpolation (using the GMT package). The result compares well with the corresponding Reynolds et al. (2002) analysis, although an average of five consecutive daily analyses (Fig. 2f) appears more similar. The

quality of the three–day and seven–day analyses can also be examined by comparing their SST spectra (Fig. 1). The *in situ* and Reynolds analyses are quite consistent down to timescales of about one month, below which the *in situ* analyses start to resolve more variance (i.e., they are noisier) than the Reynolds spectrum.

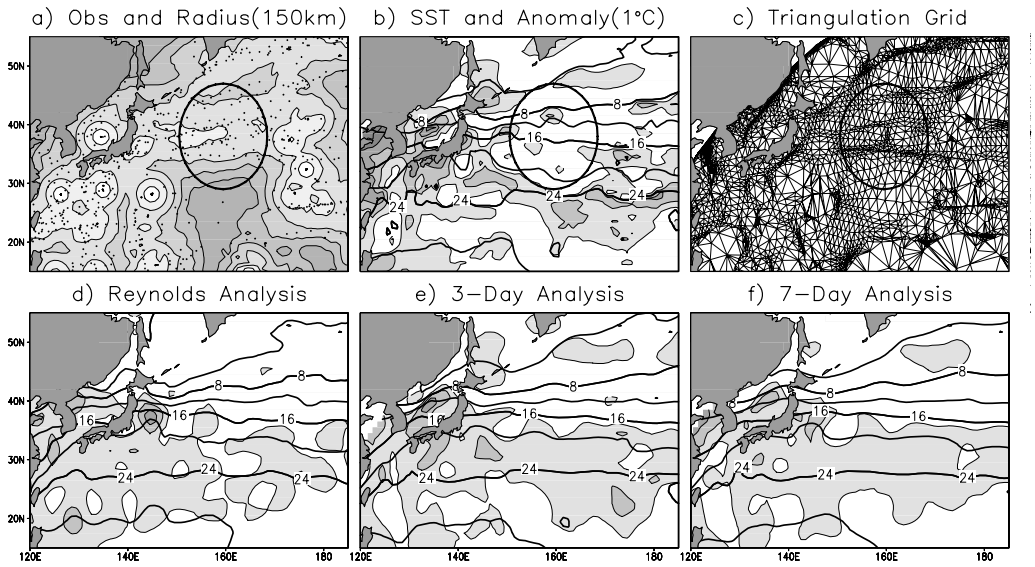

Figure 2: Example of an SST analysis based on only 810 ship and buoy observations taken on December 27–29, 1998. Shown are a) the observation positions (dots) and a spatially varying influence radius (shaded at 150 km intervals), b) interpolated SST (4°C intervals) and SST anomaly relative to a 31-year (1970–2000) average for December 28 (1°C intervals), and c) unbiased positions of the interpolated SST values in (b) (at the vertices of each Delaunay triangle). The remaining panels are as in (b), but d) the Reynolds et al. (2002) SST analysis for the week beginning December 27 and SST anomaly relative to a 19–year (1982–2000) average for December 30, e) interpolated from the triangulated grid and smoothed, and f) an average of five consecutive three–day analyses (using a total of seven days of ship and buoy observations).

A growing addition to ICOADS is metadata (e.g., measurement method) that facilitate an interpretation of the observations that have been retained. This is leading to a better understanding of systematic and random errors (e.g., Kent and Challenor 2006). In turn, this permits a physical interpretation of moderate quality *in situ* analyses. Future work will be based on the assumption that their use is appropriate for composite diagnostic studies (cf. Gyakum and Danielson 2000), in which random errors become small, but biases related to measurement method remain. The simplicity of our analysis scheme also facilitate an examination of such biases.

References

Daley, R., 1991: *Atmospheric Data Analysis*. Cambridge University Press, New York, New York, 457 pp.

Gyakum, J. R., and R. E. Danielson, 2000: Analysis of meteorological precursors to ordinary and explosive cyclogenesis in the western North Pacific. *Mon. Wea. Rev.*, **128**, 851–863.

Kent, E. C., and P. G. Challenor, 2006: Towards estimating climatic trends in SST. Part II: Random errors. *J. Atmos. Oceanic Technol.*, **23**, 476–486.

Rayner, N. A., D. E. Parker, E. B. Horton, C. K. Folland, L. V. Alexander, and D. P. Rowell, 2003: Global analyses of sea surface temperature, sea ice, and night marine air temperature since the late ninteenth century. *J. Geophys. Res.*, **108**, doi:10.1029/2002JD002670.

Reynolds, R. W., N. A. Rayner, T. M. Smith, D. C. Stokes, and W. Wang, 2002: An improved in situ and satellite SST analysis for climate. *J. Climate*, **15**, 1609–1625.

Worley, S. J., S. D. Woodruff, R. W. Reynolds, S. J. Lubker, and N. Lott, 2005: ICOADS release 2.1 data and products. *Int. J. Clim.*, **25**, 823–842.

SEA ICE MODELLING IN GLOBAL CLIMATE MODEL

V.P. Parkhomenko

Computing Centre of the Russia Academy of Sciences

Vavilov Str. 40 Moscow 119967 Russian Federation

E-mail: parhom@ccas.ru

The application of AGCM, ocean hydrothermodynamical model and sea ice evolution model to Arctic region is discussed. The purpose of the work is analysis of seasonal and annual evolution of sea ice, long-term variability of a model ice cover, and also its sensitivity to some physical and model characteristics. Results of 100 years simulations of Arctic basin sea ice evolution are analyzed. The significant (about 0.5 м) interannual fluctuations of an ice cover exist. The spectral analysis of results demonstrates 5-7 years period climate and 3-10 days synoptical ice cover fluctuations. The auto correlation function with the excluded annual and seasonal components shows data dependence with 3 days time lag. A number of numerical experiments according to influence of some physical and model parameters on results are carried out.

The ice - atmosphere sensible heat flux 10% reduction leads to growth of mean sea ice thickness within the limits of 0.05 m – 0.1 m. However in separate spatial points there is a decreasing of thickness up to 0.5 m. The maximum increase of ice thickness is observed in the end of spring and summer seasons. It is connected with the maximal difference of air - ice temperatures in the warm period.

The analysis of average ice thickness seasonal change at decreasing on 0.05 of clear sea ice albedo shows reduction of ice thickness in a range from 0.2 m up to 0.6 m, and the maximum of change is during the summer season of intensive melting. The spatial distribution of ice thickness changes shows, that on the large part of Arctic Ocean there was a reduction of ice thickness down to 1 m. However, there is also area of some growth of the ice layer basically in a range up to 0.2 m. It is located in the Beaufort Sea.

The 0.05 decreasing of sea ice snow albedo leads to reduction of average thickness of ice approximately on 0.2 m, and this value slightly depends on a season. The changes in separate points are not so great, as in the previous case, because the surface albedo change in polar areas is essential in summer period, and at this time snow on the significant areas of an ice cover has melted and does not influence on solar radiation absorption. There is a stable area of ice cover thickness increase as in previous case. Probably, it is connected with the atmospheric circulation, clouds and precipitation changes.

In the following experiment the ocean – ice thermal interaction influence on the ice cover is estimated. It is carried out by increase of a heat flux from ocean to the bottom surface of sea ice on 2 W/sq. m in comparison with base variant. Analysis demonstrates that there was a reduction of average ice thickness in a range from 0.2 m up to 0.35 m. There are small seasonal changes of these values.

The numerical experiments results have shown that an ice cover and its seasonal evolution rather strongly depend on varied parameters. The spatial and seasonal structure of changes has rather complex non-uniform character; there are great areas of opposite changes. It is connected with nonlinear behavior of feedback and interactions in model system including an atmosphere, sea ice and ocean.

This work is supported by RFFI.

Three-Dimensional Covariances of Temperature and Salinity Fields Estimated from Argo Data

Yu.D. Resnyansky, B.S. Strukov, M.D. Tsyrulnikov, and A.A. Zelenko

Hydrometeorological Research Center of the Russian Federation, Moscow, Russia

E-mail: resn@mecom.ru

The 3-D covariances of global oceanic temperature and salinity fields are estimated. Deviations of Argo measurements from the climatology WOA2001 (Conkright et al., 2002) are studied.

1. Data

Argo floats observations for the period 2005–2007 were used. The data were grouped in 10-day portions, and a simple algorithm was employed that generated super observations by averaging neighboring observations within 5-km thinning distance.

The observation data were interpolated to 21 fixed vertical levels ranged from 10 to 1400 m. The data were quality controlled with the rejection threshold $\pm 3\sigma$, with σ taken from WOA2001. The total amount of data is about 2.2×10^5 in the upper levels and 1.3×10^5 at depth 1400 m.

2. Methodology

One-point statistics (means and standard deviations) and two-point second-order moments (3-D covariances and correlations) were examined. Quasi-homogeneous regions were selected, for which the covariances were estimated relying on the local horizontal homogeneity hypothesis of the underlying temperature and salinity random fields. Without dividing the oceans into properly selected regions, spurious long-distance correlations appear, probably, due to inadequacies in the climatology used (which, in turn, may be caused by the global warming, e.g. Levitus et al., 2005). The 12 selected regions include western and eastern parts of the oceans in three latitude belts, 20°–65°N, 20°S–20°N, and 20°–65°S.

3. Results and discussion

The following conclusions can be drawn from this study (see Figs. 1–3).

1. Positive biases for temperature are apparent in the upper 1 km layer (not shown), most likely, due to global warming.
2. One-point second moments (standard deviations) for salinity monotonically decrease with depth, whereas temperature standard deviations have maximum at about 100 m depth.
3. Horizontal correlations decrease with depth from the surface down to 500–1000 m and slightly increase with depth within the layer 1000–1400 m.
4. In the Western parts of the oceans, horizontal correlations appear to be sharper – due to narrower western currents and the eddy perturbations associated with them.
5. In the near-surface layer, salinity correlations turn out to be sharper than temperature correlations (probably, due to the influence of rather spotty atmospheric precipitation field and larger-scale heat flux patterns generated by atmospheric forcing).
6. In the upper 300-400 m layer, tropical horizontal correlations, particularly in the Pacific Ocean, appear to be significantly anisotropic, with longer length scales in the zonal direction, obviously, related to the anomalies associated with El-Nino/La Nina phenomenon.
7. Vertical length scales grow with depth. Vertical correlations are, roughly, symmetric (upward vs. downward) in the z-coordinate system.
8. At the resolution provided by the Argo observational network, both horizontal and vertical correlations exhibit lack of differentiability at zero distances, implying that there is a significant amount of energy at the non-resolved scales (synoptic perturbations, jet streams, fronts).

This study has been supported by the Russian Foundation for Basic Research under grant 06-05-08076.

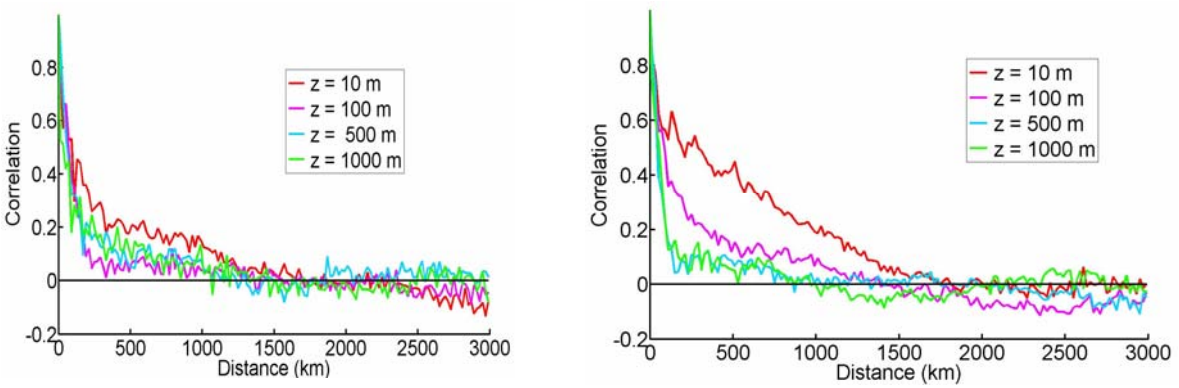

Fig. 1. North Atlantic horizontal correlations at a number of depths (see the legend): western part (left) and eastern part (right)

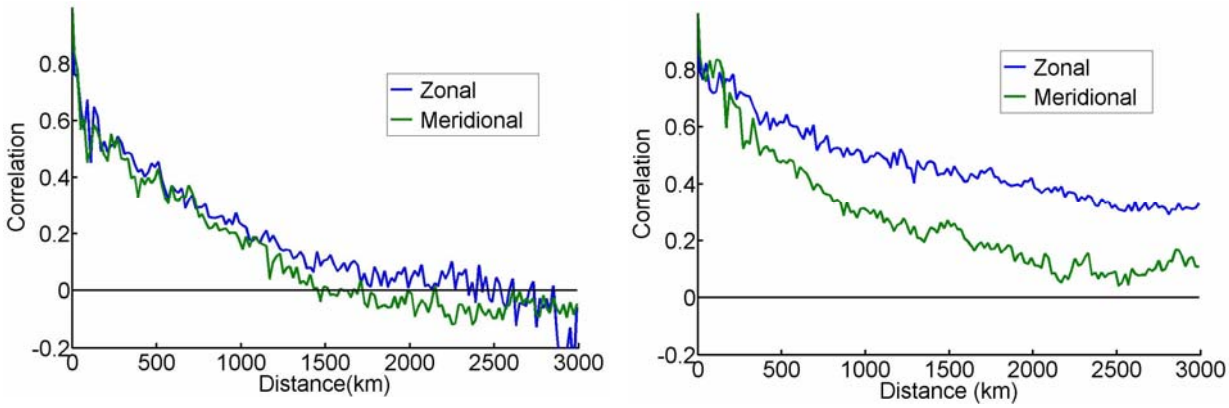

Fig. 2. Horizontal anisotropy for temperature at 10 m depth: zonal correlations (blue) vs. meridional ones (green). Left panel – Eastern North Atlantic, right panel – Eastern Tropical Pacific.

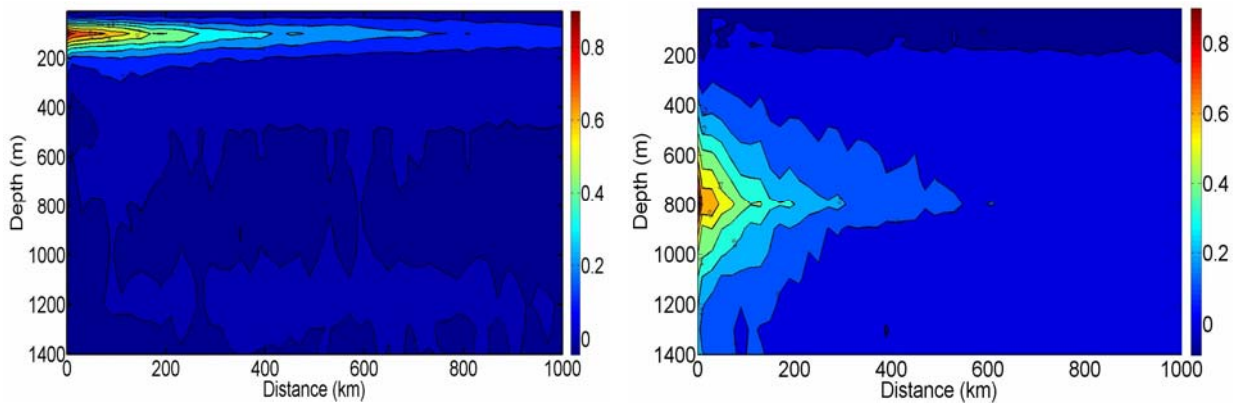

Fig. 3. Vertical cross-sections of 3-D correlations for the reference levels: 100 m (left) and 800 m (right)

References

Conkright, M.E., R. A. Locarnini, H.E. Garcia, T.D. O'Brien, T.P. Boyer, C. Stephens, and J.I. Antonov, 2002: World Ocean Atlas 2001: Objective Analyses, Data Statistics, and Figures. CD-ROM Documentation / National Oceanographic Data Center. Silver Spring, MD., 17 pp.

Levitus, S., J. Antonov, and T. Boyer, 2005: Warming of the world ocean, 1955–2003. *Geophysical Research Letters*, **32**, L02604, doi:10.1029/2004GL021592.

Chaotic behaviors of oceanic double-gyre under seasonal forcing

Shinya Shimokawa* and Tomonori Matsuura**

National Research Institute for Erath Science and Disaster Prevension, Tennodai 3-1, Tsukuba, 305-0006,
e-mail: * simokawa@bosai.go.jp, ** matsuura@bosai.go.jp

1. Introduction

The wind stress curl forces anti-cyclonic subtropical and cyclonic subpolar gyres (i.e., double gyre). Intensive western boundary currents in their gyres in each basin appear at the western flank of oceans, and enter into open-oceans as eastward jets. They carry substantial amounts of heat and momentum and strongly affect on global climate. A typical example of such currents is the Kuroshio, with 100 km width and 2 ms^{-1} velocity at maximum.

We have interested in whether the oceanic circulation itself can excite inter-annual and/or inter-decadal oscillations and also, how it is related to variations of a western boundary current. Simple models have been particularly useful in understanding various aspects of the dynamics of mid-latitude wind-driven oceanic circulation (Matsuura, 1995; Shimokawa & Matsuura, 1999; Matsuura and Fujita, 2006). Until now, they are limited to the response of oceanic circulation to a constant forcing, and the response of it to a time-dependent forcing remains to be unknown. Therefore, we focus on the response of an oceanic double-gyre to a seasonal forcing.

2. Model and Experiments

Our model is a 1.5 layer, reduced-gravity, quasi-geostrophic numerical model with a non-slip boundary condition (McCalpin, 1995). The forcing is seasonal varying in time, and north-south varying in space in the followings; $F(t,y)=-A(1.0+\alpha \cos wt)\cos(2*3.14*y/L)$. (A: the amplitude of wind stress, α: the amplitude of seasonal variation, w: the period of seasonal variation, y: the location in north-south direction, L: the length of region in north-south direction.) This represents a simplified time-space distribution of wind stress in northern mid-latitudes.

Control parameters in the experiments are b and Re number which is related to horizontal diffusion and A. We conducted the experiments in the followings; (c1) cases with a constant forcing (α=0, Re=26-314). (c2) cases with a seasonal varying forcing, (α=0.0-1.0, Re=39, 70, 112, 157, 314). We analyzed the results on flow patterns, time-series of total energy, trajectories of kinetic energy and available potential energy.

3. Results and Discussions

We would like to state the results of (c2) mainly in this paper. In cases with α=0.5 (the most realistic value), the trajectories change to chaotic (Re=39), limit-cycle (Re=70), and chaotic (Re=112) (Figure1).

In cases with Re=39, the flow pattern shows an unstable inertial sub-gyre. When b increases from 0.0, the trajectories change to limit-cycle, multiple limit-cycle, multiple torus, multi-dimensional torus, and chaos (Figure2). It is found in this case that chaotic behavior appeared with a non-linear interaction between the internal variability of double-gyre itself and the variability of external forcing. This behavior is consistent with the results in a simplified energy model (Matsuura & Shimokawa, 2007).

In cases with Re=70, the flow pattern shows a stable anti-symmetric gyre. This pattern is very stable, which is inconsistent with the results of a 2-layer shallow water model (Matsuura & Fujita, 2006). There are two possible reasons for the difference between two models in the followings; (1) a nonlinear interaction between barotropic mode and baroclinic mode in 2-layer shallow water model, (2) a asymmetry of double-gyre due to the effect of large displacement interface in 2-layer shallow water model.

In cases with Re=112, the flow pattern shows an unstable extension along north-south boundary of gyres. The changes of b seem not to affect on the results, and all the trajectories show chaos. The results with higher Re show the transition from a stable extension like laminar flow (Re=157) to an unstable extension like turbulent flow (Re=314) (Figure 3). This behavior may correspond to the transition between a non-meander path and a meander path of the Kuroshio. It is considered that the global changes of wind stress, which determines the Re and the resultant flow flux, is important in the transition of the Kuroshio.

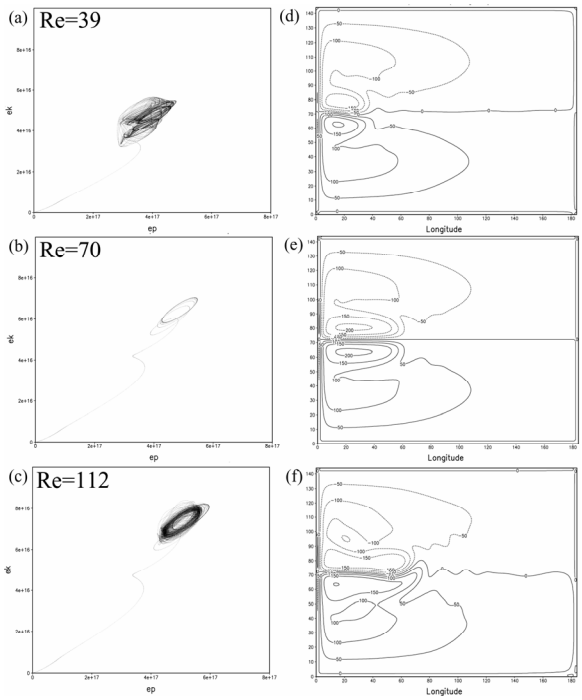

Figure 1. Trajectories of total energy and flow patterns of double-gyre (upper layer thickness at year 250) in the case with seasonal forcing (α=0.5). (a), (d) Re=39, (b), (e) Re=70, (c), (f) Re=112.

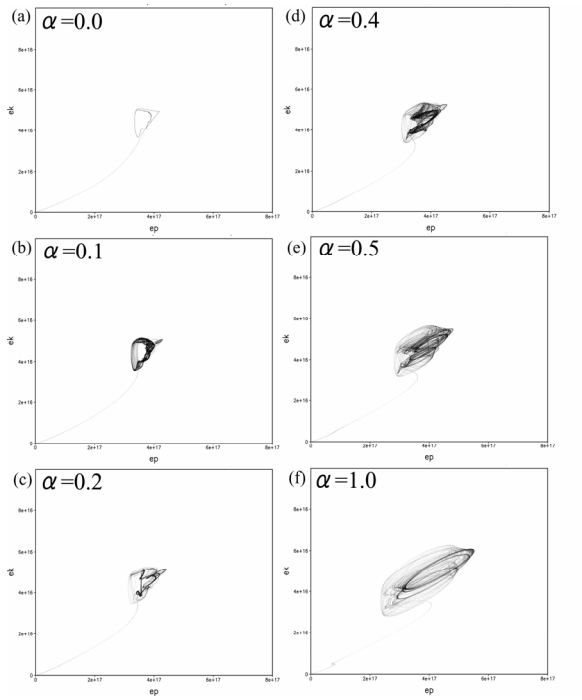

Figure 2. Trajectories of total energy in the case with seasonal forcing and for Re=39. (a) α=0.0, (b) α=0.1, (c) α=0.2, (d) α=0.3, (e) α=0.5, (f) α=1.0.

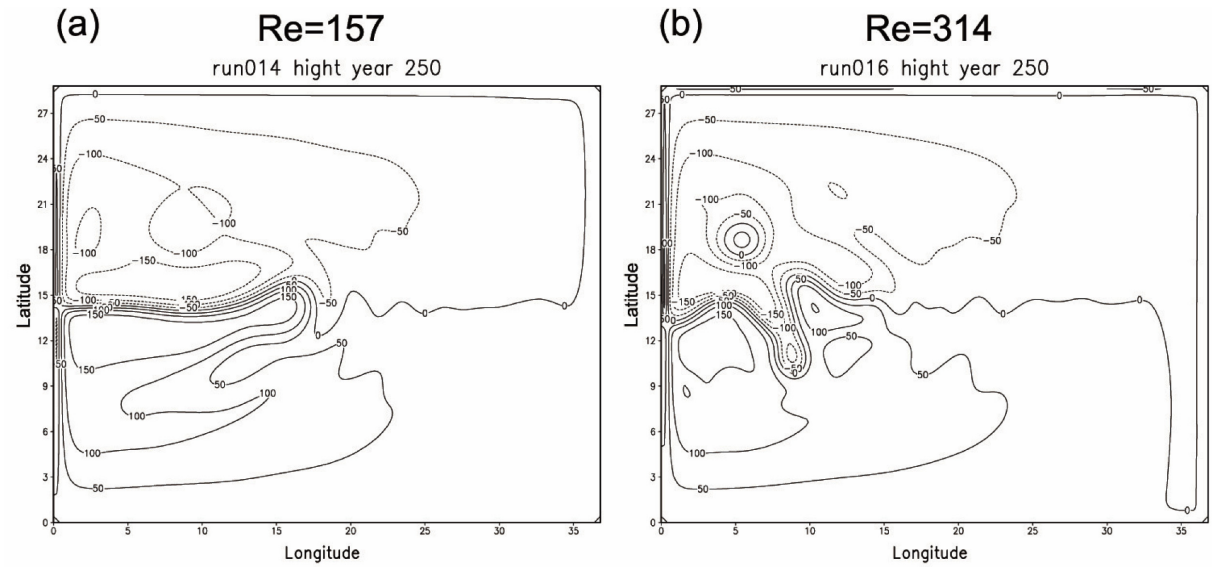

Figure 3. Flow patterns of double-gyre (upper layer thickness at year 250) in the case with constant forcing. (a) Re=157, (b) Re=134.

Refferences:

McCalpin, J. D. (1995): J. Phys. Oceanogr., 25, 806-824. Matsuura, T. (1995): J. Phys. Oceanogr., 25, 2298-2318. Matsuura, T. and M. Fujita (2006): J. Phys. Oceanogr., 36, 1265-1286. Matsuura, T & S. Shimokawa (2007): Proceedings of the Oceanogr. Soc. Japan 2007-Autumn. Shimokawa, S. and T. Matsuura (1999): J. Oceanogr., 55, 449-462.

First step towards a multi-decadal high-resolution Mediterranean sea reanalysis using dynamical downscaling of ERA40

Samuel Somot and Jeanne Colin
Centre National de Recherches Météorologiques, Météo-France.
42 avenue Coriolis F-31057 Toulouse Cedex, France, samuel.somot@meteo.fr

The Mediterranean Sea is known to show a high interannual variability in terms of deep water formation (Mertens and Schott 1998), surface circulation and other physical processes. It also experiences decadal variability as proved by the Eastern Mediterranean Transient event (Roether et al. 1996) and the existence of long-term trends in the deep layers with an increase in temperature and salinity (Rixen et al. 2005). Considering theses facts, it appears that simulating and understanding the evolution of the Mediterranean Sea over the last decades can be considered as quite a challenging task for the ocean and climate modeling community. Besides, the first scenarios of climate change applied to the Mediterranean Sea displayed a quick and strong impact on its hydrology and thermohaline circulation (Somot et al. 2006). An improved accuracy in the modeling of the past trends would give a better confidence in the model's representation of the processes implied and therefore would allow more reliable projections.

Pursuing this goal requires to work with high resolution models forced by high resolution atmospheric forcings which would follow the observed chronology. In agreement with this statement, we performed a dynamical downscaling of the ERA40 reanalysis with the ARPEGE-Climate model (Atmosphere General Circulation Model with a stretched grid, Déqué and Piedelievre 1995). This configuration has been set up running ARPEGE-Climate with its grid focused on the area of interest (50 km horizontal resolution over the Mediterranean Sea) and driving its large scales by ERA40, by dint of a spectral nudging method. The 40-year long simulation thus obtained is called ARPERA and has already been used in Herrmann and Somot (2008) for a deep convection modeling case study. Conducting the present study, we extracted the air-sea fluxes (radiative and turbulent fluxes) from this ARPERA simulation to force a Mediterranean version of the OPA model whose horizontal resolution reaches about 10 km (Somot et al. 2006). We computed the surface temperature relaxation using the ERA40 SST dataset. An additive constant correction to the climatological river runoff fluxes has been applied to obtain a realistic over-all water budget, however we let the surface salinity field entirely free. This simulation can be considered as a first step towards a 40-year reanalysis of the Mediterranean Sea in which only realistic air-sea fluxes and SST would be imposed.
The temporal evolution of the heat and salt content of the whole Mediterranean Sea, as well as the associated spatial patterns, have been analyzed using recent observed dataset (Rixen et al. 2005). Looking at the results, one can tell that the average value and the interannual variability of the heat content are well simulated by the Mediterranean model apart from a weak bias of about 0.1°C at the end of the 20th century (see figure 1 and table 1). The heat content's interannual variability of the surface and intermediate layers are very well reproduced (cf. figure 2) with time

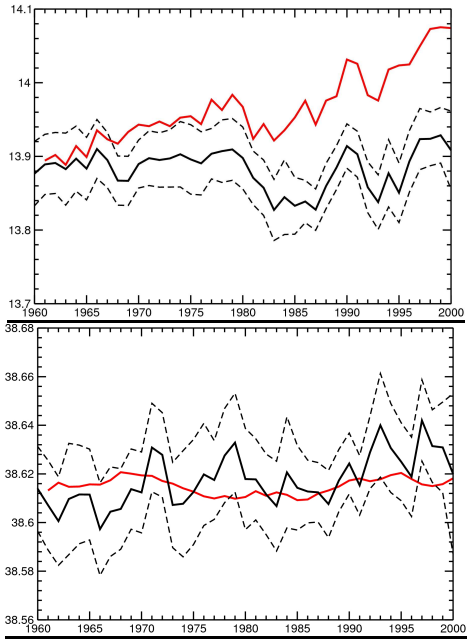

Figure 1: Time series (1 point per year) of (top) the Mediterranean Sea heat content (expressed as a 3D mean temperature in °C) and (bottom) the salt content (expressed in psu). In black, the observed values with the 2.σ range in dashed line (Michel Rixen, personal communication) and in red, the simulated values.

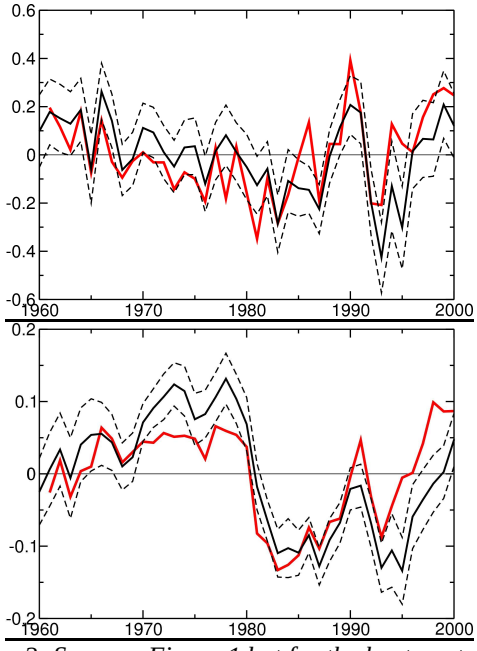

Figure 2: Same as Figure 1 but for the heat content anomaly (in °C) for (top) the upper layer (0-150m) and (bottom) the intermediate layer (150-600m).

correlations equal to 0.76 and 0.85 respectively. The decadal cold events of the 80s (Brankart and Pinardi 2001) and of the 90s (EMT, Roether et 1996) are well seen by the simulation. Concerning the salinity, only the average value is well reproduced (see figure 1) proving a deficiency in the way the sources of the salinity interannual variability are modeled.

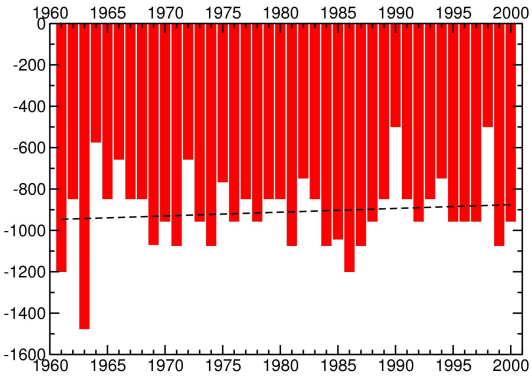

Figure 3: Time series (1 point per year) of the spatial maximum of the daily mixed layer depth in the North-Western part of the Mediterranean Sea (in m)

In the Western Basin, the open-sea deep convection and the formation of the WMDW show a realistic interannual variability (see figure 3). However no clear time correlation (not shown) is found with the observed time series (Mertens and Schott 1998) because the long-term temporal evolution of the vertical stratification appears to be too difficult to simulate without assimilating in-situ ocean data.

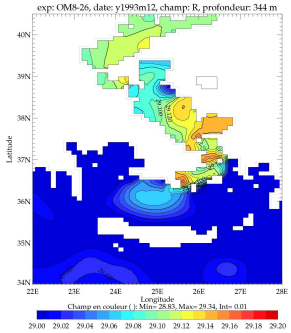

Figure 4: Density (in kg.m^{-3}) horizontal section in the Aegean Sea at a 344m-depth for December 1993 (after the main 1992 and 1993 winters of the EMT event).

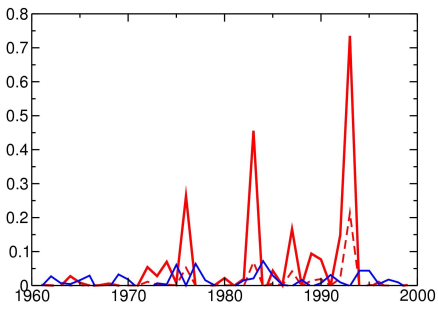

Figure 5: Yearly deep water formation rate (in Sv) in the northern part of the Aegean Sea (in red) and in the southern part (in blue). Two different density thresholds are used: waters denser than 29.10 kg.m^{-3} (full line) and denser than 29.20 kg.m^{-3} (dashed line).

Contrary to the WMDW formation, the Eastern Mediterranean Transient is mainly due to atmospheric flux anomalies and therefore is partly reproduced by our simulation without tuning the precipitation or the Black Sea freshwater input. Very cold winter and dense water formation are observed in 1993 filling the Aegean Sea (see figures 4 and 5). This newly formed water goes outside the Aegean Sea but does not sink to the bottom layer of the Levantine Basin as it actually did in reality.

1961-2000	Bias	Corr	Model trend	Observed trend
T3D (surf.-bottom)	+0.1°C	0.87	4.10^{-3} °C/yr	1.10^{-4} °C/yr
T3D (0-150m)	+0.2°C	0.76	3.10^{-3} °C/yr	-4.10^{-3} °C/yr
T3D (150-600m)	+0.6°C	0.85	-1.10^{-3} °C/yr	-4.10^{-3} °C/yr
T3D (600-bottom)*	-0.01°C	0.62	5.10^{-3} °C/yr	3.10^{-3} °C/yr
S3D (surf.-bottom)	-0.003 psu	N.S.	1.10^{-5} psu/yr	5.10^{-4} psu/yr

Table 1: Mediterranean Sea average bias (model minus observations), interannual time correlation, model trend and observed trend for the heat content expressed in °C for different layers and for the salt content in psu (: only the 1980-200 period, N.S.: Not Significant)*

In conclusion, we performed a 40-year run of the Mediterranean Sea using high resolution air-sea fluxes coming from a dynamical downscaling of the ERA40 reanalysis. In this simulation, the heat content evolution and the Eastern Mediterranean Transient event are at least partly reproduced whereas the salinity chronology and the WMDW formation process do not follow the observed chronology. In the future, improvements could be achieved by introducing interannual variability for the river runoff fluxes and for the Atlantic T-S characteristics as well as by assimilating in-situ ocean data. In forthcoming studies, this simulation will also be used as a reference to study the interannual variability of Mediterranean physical processes over the recent past years and consequently better foresee their possible evolution in the future.

References

1. Déqué M. and Piedelievre J.P. (1995) High-Resolution climate simulation over Europe. *Clim. Dyn.*, 11:321-339
2. Herrmann M. J., Somot S. (2008) Relevance of ERA40 dynamical downscaling for modeling deep convection in the Mediterranean Sea, *Geophys. Res. Lett.*, 35, L04607
3. Mertens C. and Schott F., 1998. Interannual variability of deep-water formation in the Northwestern Mediterranean. *J Phys Oceanogr*, 28: 1410-1424
4. Rixen M., Beckers J.-M., Levitus S., Antonov J., Boyer T., Maillard C., Fichaud M., Balopoulos E., Iona S., Dooley H., Garcia M.-J., Manca B., Giorgetti A., Manzella G., Mikhailov N., Pinardi N. and Zavatarelli M., 2005. The Western Mediterranean Deep Water: A proxy for climate change. *Geophys. Res. Lett.*, 32: L12608
5. Roether W., Manca B., Klein B., Bregant D., Georgopoulos D., Beitzel W., Kovacevic V. and Luchetta A., 1996. Recent changes in Eastern Mediterranean Deep Waters. *Science*, 271: 333-334
6. Somot S., Sevault F. and Déqué M., 2006. Transient climate change scenario simulation of the Mediterranean Sea for the 21st century using a high-resolution ocean circulation model. *Clim. Dyn.*, 27(7-8):851-879

Intraseasonal signals in the daily high resolution blended Reynolds sea surface temperature product and their validation over the Tropical Indian Ocean

B. H. Vaid*, C. Gnanaseelan and J. Kumar

Indian Institute of Tropical Meteorology, Pune-08, India
(*Email: bhv@tropmet.res.in)

Sea surface temperature (SST) is an important parameter in many operational and research activities, ranging from weather forecasting to climate research. In this study the new available daily SST product produced at the National Oceanic and Atmospheric Administration (NOAA) as described by Reynolds et al. (2007) has been examined. The weekly Reynolds (REY) SST product (Reynolds et al. 1994) has been widely used by various researchers though they had some drawbacks. One drawback is its inability to capture the intraseasonal variability. In this study the daily SST product is validated using the TMI and available buoy observations. Its capability to capture the intraseasonal signals has been highlighted.

The credibility of daily REY SST is quantified by computing the correlation coefficient, Root Mean Square (RMS) error and standard deviation (STD) between TMI and REY SST. The correlation between TMI and REY SST shows values above 0.8 (above 99% confidence level) over most of the tropical Indian Ocean basin. The RMS difference is observed to be less than 0.7^{o}C over the tropical Indian Ocean between 10^{o}S to 10^{o}N, most of the Arabian Sea and southern Bay of Bengal. RMS differences of the order of 0.8^{o}C are seen in the coastal regions (especially Sumatra), where the correlation is also less. STD of TMI and REY SST shows similar pattern with almost similar amplitude. To validate the daily REY SST product the continuous mooring observations at DS1 (69.3E, 15.3N), DS2 (72.5E, 10.8N), DS3 (87E, 13N), DS4 (89E, 19N) and DS5 (82E, 16N) buoys are utilized for this purpose. Figure 1 shows a comparison of SST from TMI, buoy and REY at viz five buoy locations DS1, DS2, DS3, DS4 and DS5 for the year 1998. The REY SST is comparable with the TMI and DS SST at all the five locations. At DS5, a possible warm bias in the buoy SST during the end of May was observed based on the comparison with the TMI and Reynolds data. This perhaps is due to the horizontal and temporal resolution of these products REY and TMI SST and due to their inefficiency in incorporating the rains in the algorithm. To further check the reliability of the product, Complex Empirical Orthogonal Function (CEOF) analysis has also been carried out and compared with that of TMI. The first CEOF mode of TMI and REY explains respectively 46.49% and 46.19% of the total variance. The second CEOF mode of TMI and REY explains respectively 23.19% and 18.94% of the total SST variance in the IO. So the variability (both spatial and temporal) in both REY and TMI SST showed similar pattern.

To check out the intraseasonal signals presented in the daily REY SST and TMI SST data from both the products are filtered into 10–90 day using Lanczoc band-pass filter. Figure 2 shows time series of 10–90 day SST averaged over (a) BOX1 (65E:85E,10S:3S), (b) BOX2 (80E:90E,Equator:5N) and (c) BOX3 (85E:90E,10N:14N). Intraseasonal signals of 10 – 90 days are observed to be well captured by REY and TMI SST. Saji et al. (2006) observed the cooling event in BOX1 on 27 Jan 1999, 24 Mar 1999, 25 Feb 2000, 23 Jan 2001, 29 Nov 2001, 27 Jan 2002, 07 Feb 2003, which can be seen in the intraseasonal signal of 10 – 90 days in both the products. Intraseasonal signals in TMI and REY SST in BOX2 and BOX3 are also found to be comparable.

SUMMARY

The new high resolution REY SST products is validated using TMI SST and observations from moored buoys in the tropical Indian Ocean. The most encouraging result is that, for the first time a REY SST product has become available that captures the intraseasonal signals.

ACKNOWLEDGEMENT

We thank Director IITM, Head TSD, team of daily OI SST (ftp://eclipse.ncdc.noaa.gov/pub/OI-daily), TMI SST, DS buoys. We acknowledge Mick Spillane for CEOF program and Prince K. Xavier for lanczoc band pass filter program.

REFERENCES

Reynolds, R. W. and T. M. Smith, (1994), Improved global sea surface temperature analyses using optimum interpolation. ***J. Clim.*****, 7**, 929-948.

Reynolds, R. W., T. M. Smith, C. Liu, D. B. Chelton, K. S. Casey and M. G. Schlax, (2007), Daily High-Resolution Blended Analyses for Sea Surface Temperature, ***J. Clim., 20***, 5473-5496.

Saji, N. H., S. P. Xie, and C. Y. Tam (2006), Satellite observations of intense intraseasonal cooling events in the tropical south Indian Ocean, ***Geophys. Res. Lett., 33***, L14704, doi:10.1029/2006GL026525.

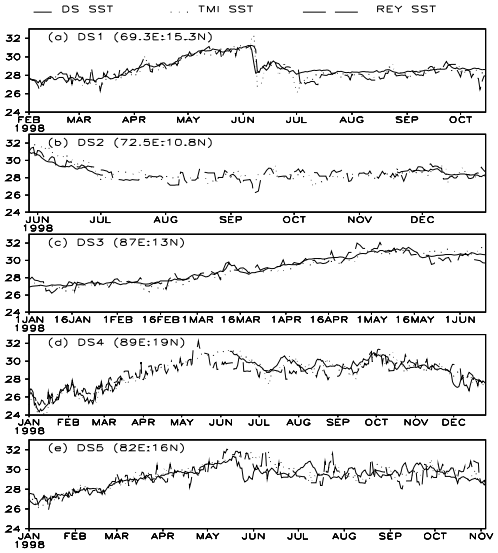

Figure 1: The comparison of TMI SST (dotted line), REY SST (dashed line) and DS SST (solid line).

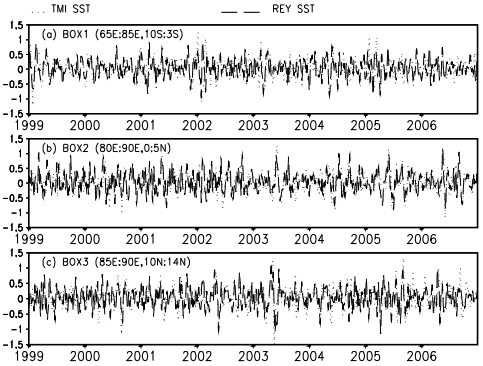

Figure 2: Time series of 10–90 days timescales intraseasonal TMI (dotted line) and REY SST (dashed line) averaged over (a) BOX1 (b) BOX2 (c) BOX3.

Sensitivity of tuning parameters in a mixed-layer scheme to simulated sea surface cooling caused by a passage of a typhoon

Akiyoshi Wada[1*], Hiroshi Niino[2], Hideyuki Nakano[1]

1) Meteorological Research Institute, Tsukuba, Ibaraki, 305-0052, Japan
2) Ocean Research Institute, the University of Tokyo, Nakano, Tokyo, 164-8639, Japan
*E-mail:awada@mri-jma.go.jp

1. Introduction

Tuning parameters in the mixed-layer scheme of Noh and Kim (1999) are usually selected to match each observation every numerical experiment. For example, a data assimilation system developed in Meteorological Research Institute/ Japan Meteorological Agency (e.g. Usui et al., 2006) has not used 'recommended values' of the parameters described in Noh and Kim (1999). If sea surface cooling (SSC) by a passage of a typhoon is affected by these tuning parameters, we need to know the sensitivity of tuning parameters to simulated SSC. Using an oceanic general circulation model, we investigated the sensitivity in the case of Typhoon Rex (1998).

2. Mixed-layer scheme and experiment design

We employed the Japan Meteorological Agency Meteorological Research Institute Community Ocean Model (MRI.COM: Ishikawa et. al., 2005) to simulate SSC caused by a passage of Rex. The MRI.COM includes a mixed-layer scheme developed by Noh and Kim (1999).

There are two arbitrary tuning parameters in Noh and Kim's mixed-layer scheme. One is a proportional coefficient associated with viscous and diffusion coefficients. The eddy viscosity K is modeled as

$$K = Sq\ell , \tag{1}$$

where q is the root mean square velocity of turbulence, ℓ is the length scale of turbulence, and S is a constant which is a function of a turbulent Richardson number defined by

$$R_{it} = \left(N\ell/q\right)^2 . \tag{2}$$

In Eq. (2), N is the Brunt-Väisälä frequency.

When the turbulent Richardson number R_{it} is relatively large, S is modeled as

$$S = S_0\left(1+\alpha R_{it}\right)^{-1/2} , \tag{3}$$

where S_0=0.39 is the value at a neutral stratification and α is one of tuning parameters.

The other tuning parameter is associated with a surface boundary condition that gives a turbulent kinetic energy (TKE) flux caused by breaking surface waves. The TKE flux may be given by

$$K_E \frac{\partial E}{\partial z} = mu_*^{\,3} , \tag{4}$$

where K_E is the eddy diffusivity, E is the mean TKE, and u_* is the frictional velocity. Here, m is one of tuning parameters.

The experiment design and atmospheric forcing has been already described in Wada et al., (2007) except that the diurnal cycle of solar radiation is taken into consideration. The pairs of tuning parameters used in the present study are shown in Table 1. The result in EXP1 was compared with the result in CNTL to investigate the sensitivity of m, while the results in EXP2 and EXP3 were compared with the result in EXP1 to investigate the sensitivity of α. The sea surface temperature (SST) observed by R/V Keifu Maru was used to evaluate the reproduction of SSC caused by a passage of Typhoon Rex (1998). The time series of SST calculated by the MRI.COM were compared with that of SST observed by R/V

Keifu Maru.

3. Results

The SST observed by R/V Keifu Maru gradually decreased accompanied with negligibly small diurnal-cycle variations, while the SSTs calculated by the MRI.COM showed more salient diurnal-cycle variations from 24 to 27 August in 1998 (Fig. 1). During the period, the sensitivity of tuning parameters to simulated SSTs was not clear among the four numerical experiments probably due to low wind speeds and small vertical turbulent mixing at the observational stationary point.

After 27 August, the SST observed by R/V Keifu Maru suddenly decreased by nearly 3°C by a passage of Rex (Fig. 1). The difference in calculated SSCs was salient from 28 to 29 August among the four numerical experiments. This reveals that calculated SSC largely depended on the value of two tuning parameters (Fig. 1). Weak surface-wave breaking (small m) and stable stratification (large α) more strongly suppressed the vertical eddy diffusion, resulting in weak SSC.

The dependency of SSC on tuning parameters is closely related to atmospheric forcing, which is necessary to run the ocean model. In the present numerical experiments, a Rankin vortex was merged into the atmospheric objective analysis dataset. Without a Rankin vortex, SSC could not be successfully calculated by the MRI.COM because wind speeds in the original atmospheric objective analysis dataset was considerably weak due to its coarse horizontal resolution. However, we show here that we need to pay attention to the values of tuning parameters even if a Rankin vortex or with a realistic wind field is introduced to atmospheric forcing.

Table 1 Experiment design of tuning parameters

experiments	α	m
CNTL	5	175
EXP1	5	100
EXP2	15	100
EXP3	2	100

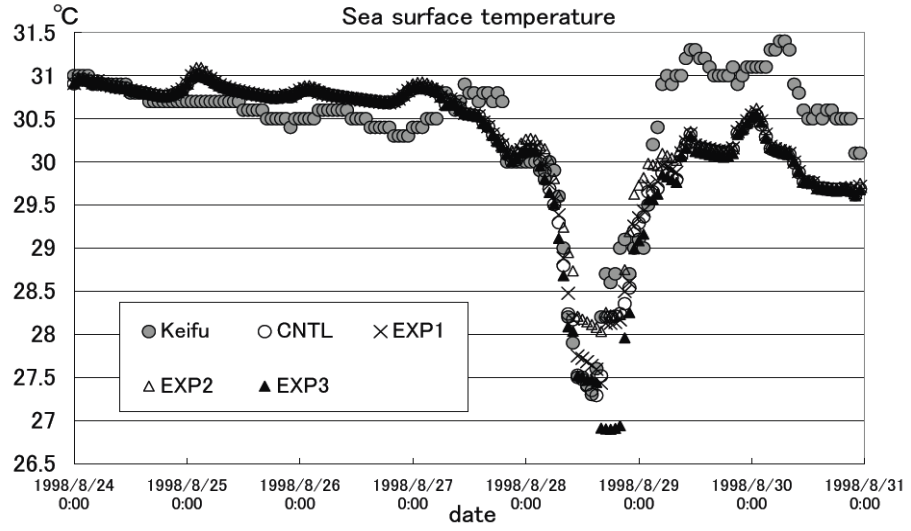

Figure 1 Time series of observed (Keifu) and simulated (CNTL, EXP1, EXP2, EXP3) sea surface temperature from 24th to 30th August in 1998 when Typhoon Rex passed around the observation area.

References

Ishikawa et al., (2005): Technical Reports of the Meteorological Research Institute, 47, 189pp. (in Japanese).
Noh and Kim (1999): J. Geophys. Res., 104, 15621-15634.
Usui et al., (2006): J. Adv. Space Res., 37, 806-822.
Wada et al., (2007) : CAS/JSC WGNE Research Activities in atmosphere and ocean modeling. 8-05.

Development of a Global Ocean Data Assimilation System

A.A. Zelenko, Yu.D. Resnyansky, M.D. Tsyrulnikov, B.S. Strukov, and P.I. Svirenko

Hydrometeorological Research Center of the Russian Federation, Moscow, Russia
E-mail: zelenko@mecom.ru

An intermittent ocean data assimilation system is being developed in the Hydrometcenter of Russia. The system provides the estimate of a current state of large scale thermohaline and dynamic fields of the World Ocean in near-real time. The assimilation is performed in a cyclic manner according to the scheme "analysis–forecast". A 2D-Var method is used at the analysis step and an Ocean General Circulation Model (OGCM) at the forecast step.

1. Data

Assimilated data are temperature and salinity observations transmitted over the Global Telecommunication System in code forms SHIP, BUOY, BATHY, TESAC. The most informative source of data is Argo floats. The typical daily amount of data is from 700 to 900 temperature and salinity profiles globally. At each analysis step, data from preceding 10 days are assimilated jointly in order to provide acceptable observations coverage. After the quality control, the data are interpolated to 21 fixed levels in the depth range 0–1400 m and are combined into super observations by averaging neighboring observations within 30 km thinning distance.

2. Forecast Model

The OGCM (*Resnyansky and Zelenko, 1992; Zelenko and Resnyansky, 2007*) is used to produce the analysis first guess fields. It is based on primitive equations with conventional approximations for modeling large scale ocean dynamic. The model includes the parameterization of small scale mixing generated by wind and buoyancy flux in the upper ocean layers, which is implemented in the framework of fully mixed-layer scheme. The model domain encompasses the global ocean except for the Arctic zone to the north of 80.3° N with the horizontal resolution 2°×2° (latitudinal steps diminishing proportionally to cosine of latitude to the north of 40° N) and 32 unevenly spaced levels in the vertical. The time step is 12 min.

The atmospheric forcing used as the upper boundary condition in the ocean model (wind stress, heat and freshwater fluxes) is taken from the NCEP/NOAA operational global forecast system, which provides data every 6-h. These fields, prescribed on Gaussian grid with horizontal resolution about 0.3°, are linearly interpolated to OGCM grid and to each time step.

3. Analysis

The 3D-Var scheme is based on a covariance (stochastic) model of the spatial auto-regression and moving-average (SARMA) type (*Tsyrulnikov et al. 2006*). A two-dimensional version of the covariance model currently used is of the spatial moving-average type. The model is defined constructively, by formulating an explicit model for the underlying forecast-error random field, ξ:

$$\xi = W\alpha ,$$

where α is the white noise and W is a discretized isotropic horizontal integral operator

$$(W\alpha)(x) = \int w(\rho(x, y))\alpha(y)dy$$

(x and y are points on the sphere, ρ is the great-circle distance) generated by an empirically selected kernel function,

$$w(\rho) = (1+\rho/L)\exp(-\rho/L)\cdot\exp[-(\rho/\lambda)^4],$$

with L being the horizontal scale parameter and λ the support-size parameter.

This model has an advantage of being positively definite with any geographically varying changes in its parameters. It can be generalized to the 3-D case and can be used for meteorological data assimilation as well.

4. Assimilation Cycle and Results

The intermittent assimilation suite produces daily analyses each of which uses observations in a sliding 10-day window. Operational assimilation started in August 2006. Before first assimilation cycle the initial spin-up model run, started from climatological WOA-2001 state, with fixed atmospheric forcing was performed. The results of the system performance are available at the Web site (http://hmc.hydromet.ru/sea/ocean/godas/godas.html). An example of the operational analysis fields is shown in the figure.

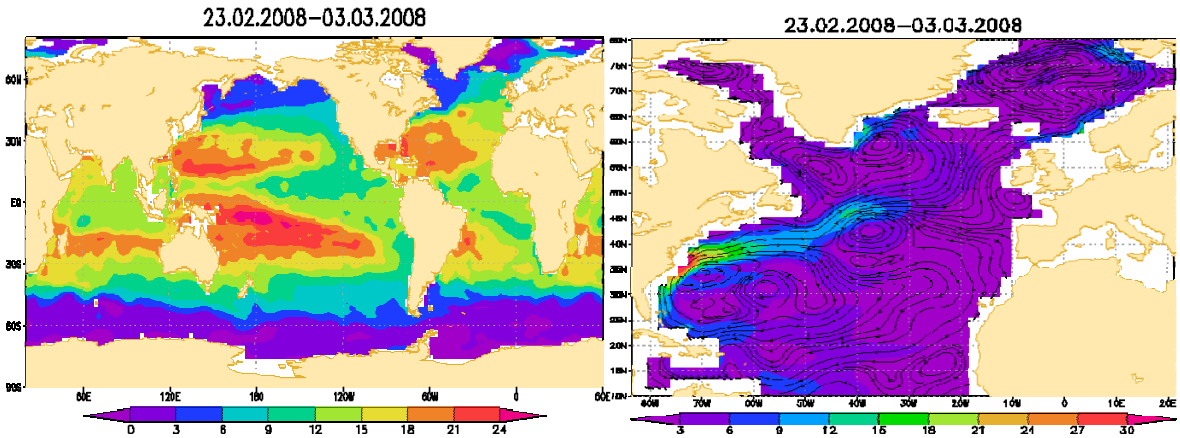

Temperature (left) and current velocity (right) analysis fields at depth 200 m averaged over 10 days period (from February 23 to March 3 2008). The magnitude of current velocity (cm/s) is presented by color scale, and current direction — by stream lines.

5. Future plans

Work on increasing the forecast and analysis resolution up to 1° in horizontal, on replacing the 2D-Var scheme by a more advanced 3D-Var scheme of the same type, and on assimilation of SST and sea surface height satellite data are underway.

This study has been supported by the Federal Program "World ocean" (subprogram ESIMO), and by the Russian Foundation for Basic Research under grant 06-05-08076.

References

Resnyansky, Yu. D., and A.A. Zelenko, 1992: Numerical Realization of the Ocean General Circulation Model with Parameterization of the Upper Mixed Layer. *Trans. Hydrometeorological Centre of the Russian Federation* [in Russian], Is. 323, pp. 3–31.

Tsyrulnikov, M.D., P.I. Svirenko, and R.B. Zaripov, 2006: Development of a 3-D Spatial ARMA-filters Based Analysis Scheme // *Research Activities in Atmospheric and Oceanic Modelling*. Ed. by J. Cote. Report No. 36. WMO/TD – No. 1347, pp. 1.39.-1.40.

Zelenko A.A., and Yu. D. Resnyansky, 2007: Deep Convection in the Ocean General Circulation Model: Variability on the Diurnal, Seasonal, and Interannual Time Scales // *Oceanology*, **47**(2), pp. 191–204 DOI: 10.1134/S0001437007020063